Heritage Science

RESEARCH

Open Access

Realizing sensations: analyzing Paul Cezanne's watercolors and assessing their light sensitivity with microfade testing

Abed Haddad*, Laura Neufeld and Ana Martins

Abstract

The exhibition *Cézanne Drawing* at The Museum of Modern Art (MoMA) brought together an exceptional group of works on paper from public and private collections across the globe. Recognizing the inherent light sensitivity of both the paper and watercolors, controlling, and tracking light exposure was central to the exhibition planning. This concern also led to a systematic study of three watercolors in the museum's collection, *Foliage* (1895), *Study of Trees* (1895), and *Mont Sainte-Victoire* (1902-06), to characterize the watercolor paints used by Cezanne in these works and their sensitivity to light exposure, and to better understand the condition of the drawings based on the palette's chemistry. Examination and analysis were undertaken non-invasively and micro-invasively with the following techniques: Infrared Reflectography (IRR), Ultraviolet Fluorescence Photography (UVF), Raman and surface-enhanced Raman (SERS) spectroscopies in addition to X-Ray fluorescence analysis on small spots and large areas using portable (p-XRF) and XRF scanning, respectively. The palette for these three watercolor drawings includes lead white, bone black, vermilion, yellow ochre, chrome yellow, emerald green, viridian, cobalt blue, and synthetic alizarin and carmine lakes. Microfade testing (MFT) was performed on the paper support and spots with each identified pigment, and the data acquired was evaluated both for color change (ΔE_{00}) and rate of color change ($\frac{\partial \Delta E_{00}}{\partial t}$). Together these techniques inform the future display and loan of these and similarly fugitive watercolors in Cézanne's oeuvre.

Keywords Paul Cezanne, Watercolors, p-XRF, XRF Scanning, Raman, SERS, MFT, Color fading, Pigment identification

Introduction

Paul Cezanne said, "painting from nature is not copying the object, it is realizing sensations," [1] a term he applied to the visual perception of color, line, and space. Though the artist is best known as an oil painter, it was on paper with graphite pencil and watercolor that he composed many of his most experimental works. Cezanne began using watercolor in the 1860s and increasingly employed the medium until his death in 1906 to capture the effects of light and atmosphere. He developed a watercolor technique that is characterized by the application of dilute, overlapping strokes of paint that are built up into vibrant layers of color and incorporate reserves of blank paper into the composition for highlights. More than 600 watercolors depicting landscapes, still-lifes, portraits, and bathers remain today [2]. The exhibition *Cézanne Drawing* at The Museum of Modern Art (MoMA) (June to September 2021) explored the artist's prolific drawing practice, bringing together more than 130 of these rarely-seen works [3].

Organizing a large exhibition of these watercolors prompted a technical study to elucidate the artist's materials and their potential response to light exposure. Three compositions in MoMA's collection were selected for analysis to evaluate their condition and light sensitivity (Fig. 1): *Foliage* (1895), *Study of Trees* (1895), and *Mont*

*Correspondence:
Abed Haddad
abed_haddad@moma.org
The David Booth Conservation Department, The Museum of Modern Art, 11 W 53rd St, New York, NY 10019, USA

Fig. 1 **a** *Foliage*, 1895, pencil and watercolor on wove paper (44.8 × 56.8 cm), Lillie P. Bliss Collection (FWN 1980); **b** *Study of Trees,* 1895, pencil and watercolor on wove paper (44.8 × 56.8 cm), Lillie P. Bliss Collection (FWN 1405); **c** *Mont Sainte-Victoire*, 1902–06, pencil and watercolor on wove paper (42.5 × 54.2 cm), Gift of Mr. and Mrs. David Rockefeller (FWN 1504). All three works are in the collection of The Museum of Modern Art

Sainte-Victoire (1902-06). The first two are executed on the same support, with *Foliage* on the recto and *Study of Trees* on the verso, which was a common practice for the artist [2]. These compositions were chosen because they share the palette and woven paper supports that are characteristic of Cezanne's mature works [4]. As the artist's technique evolved, his watercolor palette and selection of paper supports became more refined and consistent [5]. This allows for the extrapolation of analytical results to other watercolors by the artist from the same period (1880s-1906).

The material qualities that define Cezanne's watercolors, luminous paint on bright paper, also make them vulnerable to light. Executed more than one hundred years ago, many works now display varying degrees of discoloration. Most apparent is the darkening of paper supports, the fading or darkening of emerald green in dilute passages, and the dulling of organic reds [5]. Watercolor and gouache are traditionally classified as sensitive to light [6–8], and the literature indicates that water-based paints can differ in their lightfastness [9–11]. Previous research by Zieske [12, 13] investigated the pigments and papers used by Cezanne in nine watercolors in the collection of the Philadelphia Museum of Art (PMA) executed between c. 1877 and 1904, where the following pigments were identified by energy dispersive X-ray spectrometry (EDS): lead white, vermilion, red lead, iron oxides, chrome yellow, emerald green, viridian, and cobalt blue; ultramarine and organic pigments were inferred based on the absence of other detectable elements and the observed color. Later research carried out by Reissner [14] and Burnstock et al. [15] on five watercolors in the collection of The Courtauld Gallery indicated a similar consistency in pigment choices save for one instance of indigo found in *Still Life with Apples, Bottles, and Chairback* (1904-06). It is important to note that parallel research into Cezanne's oil palette has been conducted by these and other institutions but is outside the scope of this study, even though there are similarities between the artist's pigment choices in both media [14–17]. Many of Cezanne's extant sketchbooks (FWN 3000, 3002, 3005, 3007–10, 3015, and 3018) include lists of pigments and art materials (see example in Fig. 2) [2]. These notations, alongside references made in letters to color merchants, served as primary sources of information about his preferred pigments, which included lead white, earth pigments, vermilion, organic reds (alizarin and

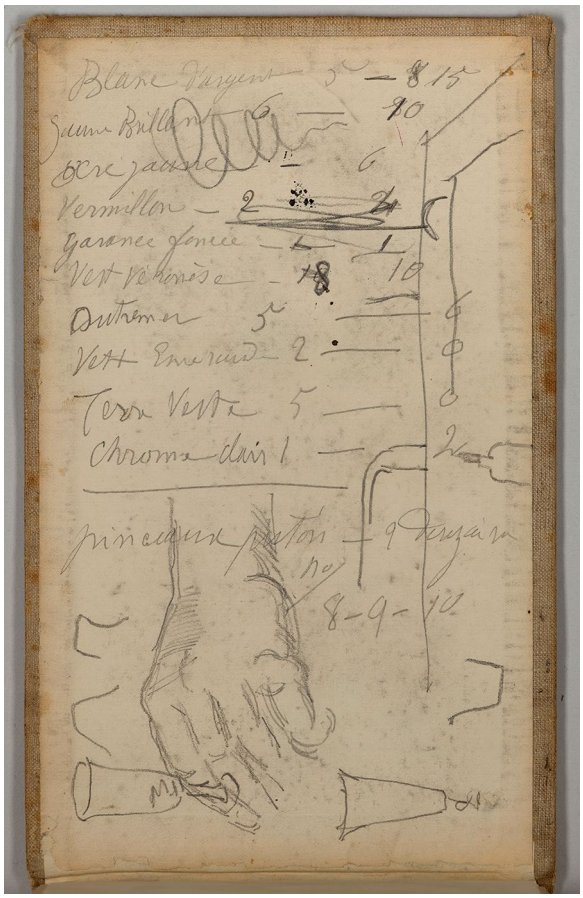

Fig. 2 Pigments listed in *Sketch of a hand and notations*, 1879–82. Graphite on wove paper, front endpaper from the New York sketchbook. 5 × 8 9/16 in. (12.6 × 21.7 cm). The Morgan Library & Museum, New York. Pigments include emerald green (*vert Veronese*), viridian (*vert emeraude*), green earth (*terre verte)*, madder lake (*garance foncée*), vermilion (*vermillon*), cobalt blue (*bleu cobalt*), ultramarine (*outremer)*, ochre (*ocre jaune*), Naples yellow *(jaune brilliant),* chrome yellow (*chrome clair*), and lead white (*blanc d'argent*)

carmine-based), chrome yellow, Naples yellow, emerald green, viridian, cobalt blue, and synthetic ultramarine.

In this work, each drawing was visually examined with normal and raking illumination, under magnification with a binocular microscope, and through photo documentation with ultraviolet-induced visible fluorescence (UVF). This was done to assess the physical condition of the media and paper supports and elucidate the artist's working methods. Identifying the pigments used was essential for characterizing their response to light exposure. Pigment analysis was conducted non-invasively using portable X-ray fluorescence (p-XRF) and large area X-ray fluorescence scanning, and micro-invasively using Raman and surface-enhanced Raman spectroscopy (SERS). After pigment identification, microfade testing (MFT) was done to gauge the light sensitivity of the watercolors in their current state. The use of MFT on watercolors has become a relatively common practice [10, 11, 18–21] to better assess the light sensitivity of what has been traditionally considered one of the most light-sensitive media.

Methods and materials

Imaging

UVF Photography was carried out according to the UV Innovations workflow with a Canon EOS 5D Mark II (Zeiss Mak-ro-Planar T* 2/50 ZE lens). The standard infrared filter was replaced by a 2E and a Peca #918 UV-blocking filters. UV irradiation was provided by two Altman Spectra Cyc UV lamps, a 100 W cyclorama/wall wash luminaires with high output 365 nm UV LED emitters. The camera was calibrated with an X-rite ColorChecker Passport and a UV Innovation Target-UV™.

Surface microscopy was carried out using low-power magnification Wild Heerbrugg binocular microscope with a 6–200 × magnification range and illumination using a fiber-optic light source Schott ACE 1 at 3250 K color temperature. Images were captured using a Canon EOS Rebel T3I with an Optem 1.6 × t-mount adapter. All microscopic images of the surface were white-balanced in Adobe Photoshop 2021. UVF surface microscopy was performed in the previously described manner with irradiation provided by a portable Reskolux UV 365 flashlight, UV-A spectrum 360–370 nm. The camera was calibrated with a UV Innovation Target-UV™.

Instrumental analysis

Portable, handheld X-ray fluorescence (p-XRF) was carried out using a Bruker Tracer 5i operated at 40 kV and 4.5 μA; spectra were acquired without He purge using the Bruker Artax 8.0 software for 120 s and the 8 mm collimator. Several spots of similar colors were acquired for each drawing and the data was further examined with the Bruker Artax 8.0 software.

Large area XRF scanning was carried out using a Bruker M6 JetStream with a Rh target and SSD detector at 50 kV and 600 μA, with a 550 μm spot size, 550 μm pixel size and dwell time of 10 ms/pixel. The spectra were visualized using the Bruker M6 Jetstream software and further processed by employing a combination of PyMca [22] and Datamuncher software [23] to obtain elemental distribution maps.

Raman spectroscopy was carried out on micro samples using a Renishaw In-via Raman system equipped with a 785 nm diode laser operated between 0.3 to 3 mW, a 1200 lines/mm grating, and a Leica confocal microscope with a 50 × LWD or 100 × objective. Final

spectra represent an average of five acquisitions of 10 s. Spectra were examined using the Spectral Search and Multicomponent Search tools available in the Thermo Scientific OMNIC Specta 2.0 software and compared to published spectra in spectral databases [24–26].

Silver nanoparticles (AgNPs) for surface-enhanced Raman spectroscopy (SERS) were prepared according to a method developed by Lux et al. [27]. A solution of 12.5 mL of 0.5 mM silver sulfate (Ag_2SO_4) ($\geq$ 99.99%), 0.5 mL of 1% sodium citrate dihydrate ($C_6H_9Na_3O_9{\cdot}2H_2O$) ($\geq$ 99%), and 1 mL of 1% D-glucose ($\geq$ 99.5%) are mixed in a Hydrothermal Synthesis Autoclave Reactor PTFE Tank (Baoshishan, China) previously cleaned with nitric acid at 30%. Once closed, the vessel was positioned in the center of a Panasonic model NN-SD372S inverter microwave and heated at 810 W for 2 min. 1.5 mL aliquots of this stock solution of citrate-capped AgNPs were centrifuged at 12,000 rpm for 15 min. The supernatant containing the citrate solution in excess was removed and replaced by distilled water to avoid sodium citrate interference in the SERS spectra. The sample was pretreated with HNO_3 to hydrolyze any lakes present into the colloidal solutions by breaking the bonds with the base onto which the dye was precipitated. All chemicals were purchased from Millipore-Sigma, USA. SERS was carried out using the same Renishaw In-via Raman system with a 532 nm diode laser operated at 0.25 mW. Spectra were also evaluated using Spectral Search and Multicomponent Search tools available in the Thermo Scientific OMNIC Specta 2.0 software.

MFT was carried out using an Instytut Fotonowy automated microfader fitted with a 3000 K LED light source operated at 900 µA over 600 s and a spot size of 550 µm for a total exposure of 1.65 Mlx·h. Blue wool standard (BWS) cards were purchased from Talas (USA) and were used as received. The color change was reported using the CIE Lab ΔE_{00} equation. Data was acquired using the Instytut Fotonowy MFT software version 2.0 and further examined using Origin 2022 Pro from OriginLab. Eighteen representative areas for the distinct colors identified and paper support across the three works were chosen and three replicates were done per area, slightly moving the drawing to a new spot with each measurement. For colors, saturated passages that appeared pure, instead of thinner washes, were chosen to minimize the contribution of the paper support to the total color change measured.

Results and discussion

Paper supports

The selected works are executed on moderately thick, slightly textured, semi-absorbent wove supports [28]. The sheet dimensions and irregular edges indicate they are likely on French *raisin* format papers that have been slightly trimmed [29]. *Raisin* papers measure approximately 48 × 63 cm with slight variation in the dimensions based on the manufacturer, system of measurement, and between handmade and machine-made papers [30, 31]. *Foliage* and *Study of Trees* share a cream-colored sheet that bears no manufacturer's mark. The paper displays varying degrees of darkening likely due to exposure to both light and atmospheric pollutants. On *Foliage* (recto), minor overall light induced darkening mutes the luminosity and contrast of the thinly applied colors. *Study of Trees* (verso) displays more pronounced darkening, especially along the edges of the paper, from previous contact with an acidic mount and framing materials.

Mont Sainte-Victoire is on a white paper that retains a bright, even tonality, imparting vibrancy to the colors. An impressed watermark reading CANSON & MONTGOLFIER SAINT MARCEL LES ANNONAY is visible along the top edge of the support. The French mills of Canson and Montgolfier were renowned for their production of artist papers, and their manufacturer's marks are visible on many of Cezanne's mature works [4, 5]. Fiber analysis conducted by Zieske on a watercolor drawing from the same period and with the same impressed mark was found to contain only linen and cotton rag fibers [13]. The physical qualities of the sheet used for *Foliage* and *Study of Trees*, including its degree of discoloration and embrittlement, are consistent with the qualities of sheets at the PMA containing both rag and non-rag fibers, including grass and wood [13]. These supports may be more prone to discoloration due to the type of fibers, the pulp processing methods employed, or the type and proportion of sizing and additives used, such as alum and rosin, which can have deleterious effects on the long-term stability of the paper [32, 33]. The acidity of the paper supports was not assessed due to the invasive nature of the analysis.

The palette

Analysis was first conducted non-invasively using p-XRF to characterize the watercolor palette. Even though this technique proved challenging due to the extensive overlap in paint application and the double-sided nature of *Foliage* and *Study of Trees*, the analysis identified the presence of emerald green (Cu, As), cobalt blue (Co, Al), yellow and red ochres (Fe, Al, Si, K), yellow and/or orange lead chromates (Pb, Cr), vermilion (Hg), red lakes (indicated by the absence of inorganic markers), and possibly bone black (Ca, P); the palette appears similar for all three works. Analysis of *Mont-Sainte Victoire* using XRF scanning proved useful for visually separating the

overlapping paints and confirming the pigments above. Previous technical studies conducted at the PMA and the Courtauld Institute, also by p-XRF [12, 13, 15], identified the same watercolor pigments found in the three MoMA drawings. A comparison with the artist's annotations on pigments in his sketchbooks (Fig. 2) also supports the remarkable consistency of his palette, albeit it is unclear whether they relate to oil paints or watercolors.

Interpreting Cezanne's notations, however, must be done with caution in relation to the green pigments. Veronese green and emerald green are somewhat confusing terms; copper acetoarsenite was marketed in England under the name emerald green, but in France, "vert emeraude" was already in use to describe viridian (or hydrated chromium oxide), and copper acetoarsenite was sold as "vert Veronese" as a result [12, 34]. A sample taken from the work and analyzed with Raman spectroscopy confirmed that the UV-absorbing pigment was copper acetoarsenite ($Cu(C_2H_3O_2)_2 \cdot 3Cu(AsO_2)$ (107, 121, 154, 176, 243, 239, 296, 327 433, 495, 542, 762, 834, and 952 cm^{-1}) [35]. UV proved to be a simple and effective tool for identifying and assessing the condition of emerald green, or copper acetoarsenite, as even thin or degraded passages strongly absorb UV radiation [36]. In *Mont Sainte-Victoire*, this absorbance evidenced two horizontal brushstrokes in the sky where the green hue is now nearly imperceptible (Fig. 3).

While the degradative action of the pigment on paper supports is inconclusive it has been observed to sometimes protect the fibers from darkening [28, 31, 32]. This is seen on the double-sided sheet with *Foliage* and *Study of Trees* where passages of emerald green on the recto, have locally mitigated the darkening of the paper on the verso (Fig. 4). Strokes of emerald green on the recto in *Foliage* correspond to areas on the verso in *Study of Trees* that are lighter in tone than the surrounding paper. This condition has been observed in other works by the artist by Zieske in some PMA watercolors, particularly those executed on paper sheets that contain more non-rag fibers and display noticeable darkening as a result [13].

XRF scanning of *Mont Sainte-Victoire*, which mapped the distribution of the elements in the pigments across the composition, was particularly useful for distinguishing between emerald green and viridian (Fig. 5). This was the only drawing chosen for XRF scanning since *Foliage* and *Study of Trees* are executed on the same support rendering interpretation challenging. The map for copper shows Cezanne's prevalent use of emerald green, while the map for chromium displays his selective and spare use of viridian in strokes that punctuate the landscape and base of the mountain. Chromium is found

Fig. 3 Details of *Mont Sainte-Victoire* under normal **a** and UV illumination **b** that show the extent of fading of the emerald green clouds in the sky (outlined in green lines), which remains visible under UV. The orange fluorescence is the result of staining, the source of which is currently unknown

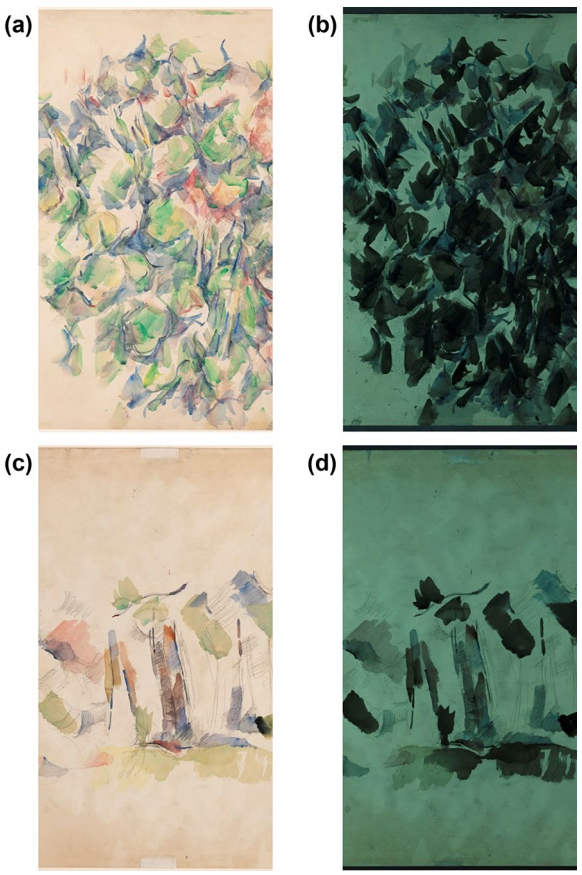

Fig. 4 Details of *Foliage* **a**, **b** and *Study of Trees* **c**, **d** under normal **a**, **c** and UV **b**, **d** illumination, illustrating the protective effect of emerald green (UV-absorbent dark stroked) on the paper, which appears mottled in *Study of Trees* because of the more densely executed *Foliage*. The images for *Study of Trees* are mirrored to illustrate this effect

with lead in some yellow brushstrokes possibly indicating the presence of lead chromate. The lead map also shows that Cezanne sometimes added lead white to a pigment to lighten its hue and increase the opacity of the watercolors. Other maps are also illustrated in Fig. 5: cobalt for cobalt blue, iron for ochres, and mercury for vermilion.

Beyond confirming the palette, XRF scanning illuminates Cezanne's method of paint application, which the artist Emilie Bernard called "excessively complicated." In 1904, Bernard watched Cezanne work on a watercolor of *Mont Sainte-Victoire* and described his process of slowly applying discrete but overlapping brushstrokes "until all these colors, like folding screens, modeled and at the same time colored the object" [37]. In isolating each element and thus pigment, the maps provide insight into the artist's distinctive technique (Fig. 6).

To further clarify the nature of the organic red pigments, micro samples were taken from the drawings to be analyzed with Raman and SERS (Fig. 7). To the authors' knowledge, this is the first fingerprint identification of red organic lakes used by Cezanne in watercolors. Alizarin lake was detected in *Mont Sainte-Victoire* using Raman spectroscopy (241, 485, 675, 844, 904, 964, 1021, 1164, 1192, 1222, 1294, 1329, 1331, 1481, 1522, 1578, and 1634 cm^{-1}) [25], and carmine lake was detected in *Foliage* using SERS (372, 797, 1074, 1229, 1300, 1457, 1571, and 1641 cm^{-1}) [26]. Anhydrite ($CaSO_4$) was detected in the lake sample from *Foliage* by Raman spectroscopy, with a characteristic $\nu_1(SO_4^{2-})$ stretching mode at 1007 cm^{-1} [38] and is present as a filler [39]. Moreover, based on the lack of fluorescence under UV [8, 40], the lakes appear to be synthetic in origin, which is likely, given that synthetic alizarin and carmine lakes were available commercially by the late nineteenth century [41]. The absence of UV-induced fluorescence was also observed by Zieske et al. in other watercolors by Cezanne [12, 13].

The observation of fluorescence in a fourth work considered for the exhibition, *The Bridge at Gardanne* (1885–86), prompted assessment for the presence of a possible natural lake (Fig. 8). Surprisingly, rhodamine 6G was detected, a synthetic organic dye patented by Maurice Cresole in 1892 [42], several years after the current dating range of *The Bridge at Gardanne*. However, it is important to note that the dating of Cezanne's works is often uncorroborated as he rarely signed his watercolors [2], and further research is required to better situate this drawing within his oeuvre. Rhodamine 6G was identified by SERS (Fig. 7) (xanthene ring puckering mode, 609 cm^{-1}; C–H out-of-plane bend, 770 cm^{-1}; C–H xanthene ring in-plane bending, 1180 cm^{-1}; C–H aromatic

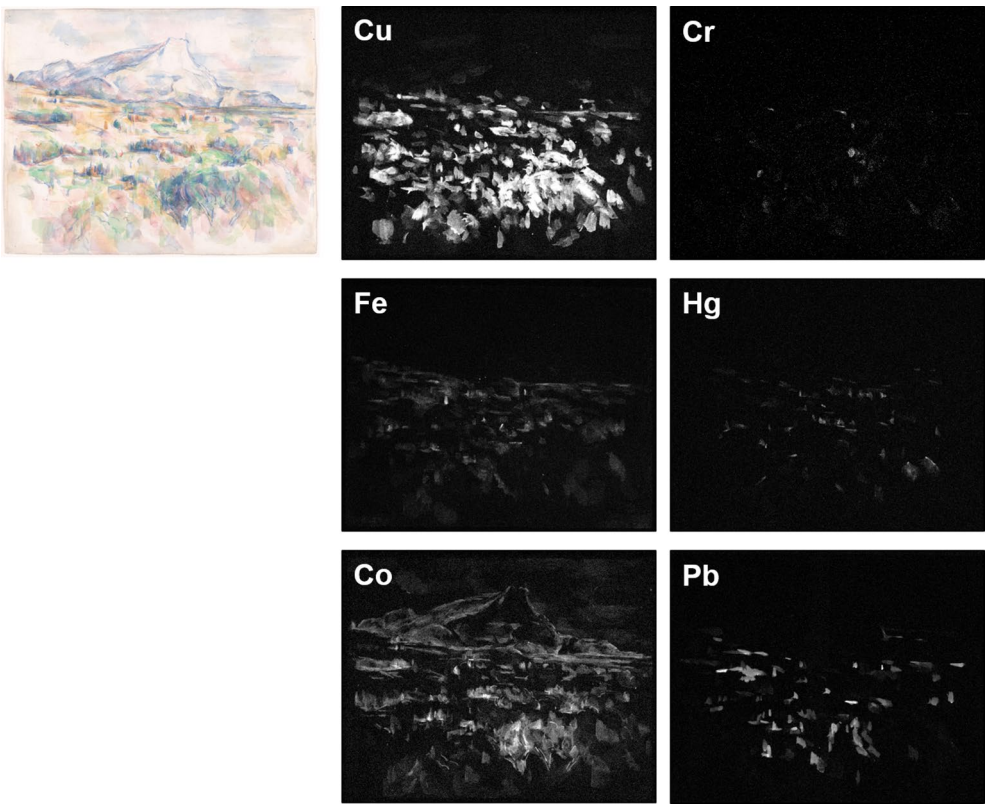

Fig. 5 Elemental distribution maps of *Monte Sainte-Victoire* obtained with XRF scanning

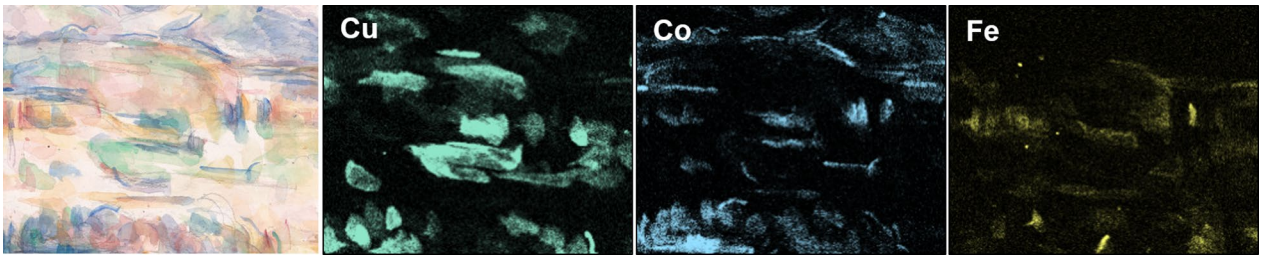

Fig. 6 Elemental distribution maps for a detail from *Monte Sainte-Victoire* obtained with XRF scanning that illustrate how, for example, emerald green (Cu), cobalt blue (Co), and yellow ochre (Fe) are applied in distinct, overlapping brushstrokes

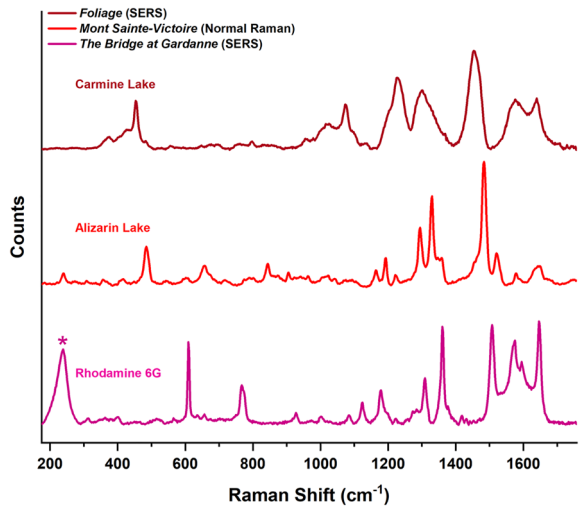

Fig. 7 Raman and SERS spectra of red samples taken from *Foliage*, *Mont Sainte-Victoire*, and *The Bridge at Gardanne*. The * indicates the Ag–N bond

bends, 1310 cm^{-1}; aromatic C–C stretch, 1360 cm^{-1}; aromatic C–H bends, 1508 and 1570 cm^{-1}; and Aromatic C–C bend and C=C symmetric stretch, 1647 cm^{-1}) [43] alongside larger granules of vermilion (A_1 mode at 256 cm^{-1}, E_2 LO mode 286 cm^{-1}, and E_1 TO mode at 346 cm^{-1}) [44] by normal Raman. A strong peak at 238 cm^{-1} in the SERS spectrum indicates chemisorption of the dye to silver nanoparticles through an Ag–N bond otherwise unobserved in normal Raman spectra for nitrogenous compounds [45]. Rhodamine 6G also has an excitation maximum that lies around 541 nm. The use of an excitation wavelength of 532 nm for SERS exploits that transition and permits detection at concentrations on the single molecule level with colloidal silver nanoparticles [46].

This finding is similar to the detection of a mauveine lake by SERS used in *The Miracle of the Slave* (1850–1860), an early painting attributed to Cezanne in the collection of the Muscarelle Museum of Art, soon after its synthesis [17]. Synthetic lakes based on eosin, mauveine, and methyl violet were available to French artists in 1890 as advertised in a Lefranc et Cie catalog [47], although artists were cautioned about the sensitivity of synthetic lakes to light [48]. It is also quite possible that rhodamine 6G was added to vermilion by late-nineteenth-century paint manufacturers, considering the common addition of synthetic organics as adulterants and toners [47].

Microfade testing

The colors and locations tested were based on the pigment analysis and included the organic reds, emerald

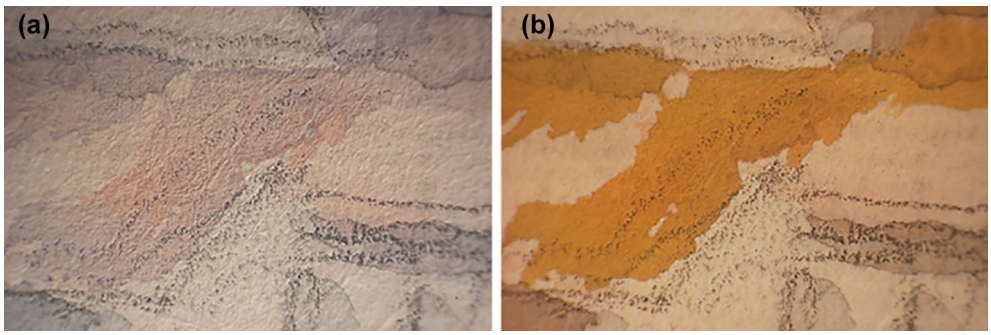

Fig. 8 Normal (left) and UV (right) micrographs of a dull red watercolor seen in *The Bridge at Gardanne* that shows the degree of fluorescence exhibited by partially faded rhodamine 6G

green, cobalt blue, and yellow ochre for all three drawings; vermilion, which appears orange, was only readily accessible in *Study of Trees* without significant overlap from other colors. The paper was also tested, and areas that appeared least discolored were chosen for analysis with MFT. The resulting color change curves (ΔE_{00}) were corrected using a normalization procedure proposed by Mecklenburg et al. [49], and used in this case to account for variations in pigment concentration, thickness in the watercolor application, and surface texture from the paper fibers. This normalization method builds on previous research into the kinetics of colorant fading described by Giles et al. as Type II fading [50], where the change in ΔE is initially rapid and followed by change at a slower and constant rate. This procedure builds on work by Daniels that separates fading rate constants, which are physical and color-based, and reaction rate constants, which are chemical and concentration-based [51].

In this mathematical model, each set of curves was normalized to the ΔE_{00} curve showing the fastest change to approximate the most conservative estimate of lightfastness. This model relies on the research described by Giles, Johnston-Feller, and Daniels above where the fading of most colorants can be described in terms of a power function:

$$f(x) = kx^n$$

Where *f(x)* stands for the color change in ΔE_{00}, *x* is the time, and *k* is a constant; *n* is a real number. In general, *n* values may vary from 0.1 to 0.5 for MFT curves, increasing in value from least to most fugitive [49].

Normalization starts by taking the first derivative of the fastest and slowest fading curves with respect to time ($\frac{\partial \Delta E_{00}}{\partial t}$) and adjusting the latter to the former by identifying the shift in the x-axis (time in sec) needed to align the first data points. The curve is then shifted in the y-axis (ΔE_{00}) to align the curves at the 60-s mark, a point at which the steep rate of change during the initial measurement period for Type II faders becomes more constant or plateaus. A correction factor is then obtained by dividing the shift in the x-axis by that in the y-axis and multiplying the ratio by a factor of -2. The last step reflects the fading behavior of most light sensitive materials for the power function above, where $e^{-0.5}$ describes the derived fading curve. The correction factors are listed for each color examined with MFT in Additional file 1: Table S1 of the Supplementary Materials. As an example, normalization for MFT curves from three yellow ochre spots in *Study of Trees* is illustrated in Fig. 9.

Overall, this normalization procedure shifts the curve in both time (x-axis) and ΔE_{00} (y-axis), resulting in superimposed curves that are similar in their final value, i.e., at 600 s in this measurement campaign. The superimposable nature of these curves suggests they are curve segments of a single fading behavior, one that is isolated from the effects of the initial L, a, and b values in CIE L*a*b* color space at t_0 during an MFT run. After normalization, the curves for each trial were then fitted to a concatenated power function to further reduce the effect of surface inhomogeneity in lieu of averaging. The exponent b in the power function of the fittings was close to between 0.3 and 0.5 for all samples, expressing behavior similar to a square-root power function, or Type II behavior. The fitted curves all reported high R^2 values between 0.86 and 0.99 (Additional file 1: Figs. S1–S3), indicating an overall good fit. The reported ΔE_{00} values represent this normalization procedure done on three trials per color and paper substrates (Table 1) and the MFT-induced color change curves over 600 s are additionally illustrated in Fig. 10.

With ΔE_{00} at 600 s secured, the rate of change was then extracted using a method proposed by Prestel [52]. In brief, the first derivative of each fitted ΔE_{00} curve is calculated and the value at the end of each differentiated curve is representative of a rate of change that corrects for the rapid discoloration observed initially in materials that exhibit Gilles Type I and Type II behavior (Table 1). The differentiated curves for the other spots are similar in shape to those in the inset of Fig. 9a. Elucidating both the values for ΔE_{00} and $\frac{\partial \Delta E_{00}}{\partial t}$ allows for a holistic description of the behavior exhibited by the areas chosen by plotting them together (Fig. 11).

Categorical boundaries for BW1, 2, and 3 were defined by calculating mean values between successive BWS, for both ΔE_{00} and $\frac{\partial \Delta E_{00}}{\partial t}$, which allows for classification of colorants based on both absolute change and rate of change [52, 53]. This compensates for the discrepancy between measurements by removing factors such as pigment concentration, surface texture, and possibly exhibition history. For example, the ochres and emerald greens from different spots and drawings group better within the BW3 boundaries (Fig. 11c) when accounting for both metrics.

Most spots analyzed were classified as BW3, with the paper of *Study of* Trees and carmine lake classified as BW2. Only the carmine lake in both *Foliage* and *Study of Trees* is predicted to approach or surpass a just noticeable difference (JND) of $\Delta E_{00} = 1.5$ [49, 50, 54] after 1.65 Mlx·h of exposure. The sensitivity of carmine lake in water colors was indicated as early 1888 by Russel and Abney [6, 7]. Examining the curve in Fig. 10b for the carmine lake in *Foliage* ($\Delta E_{00} = 1.7$), it would take approximately 483 s, or 1.2 Mlx·h to achieve JND, which translates to ~ 3000 days (~ 8 years) of exhibition days at 50 lx for eight hours a day, similar to the decadal lighting dose of 1 Mlx·h established by Ford at the National Museum of Australia for BW2 materials illuminated at

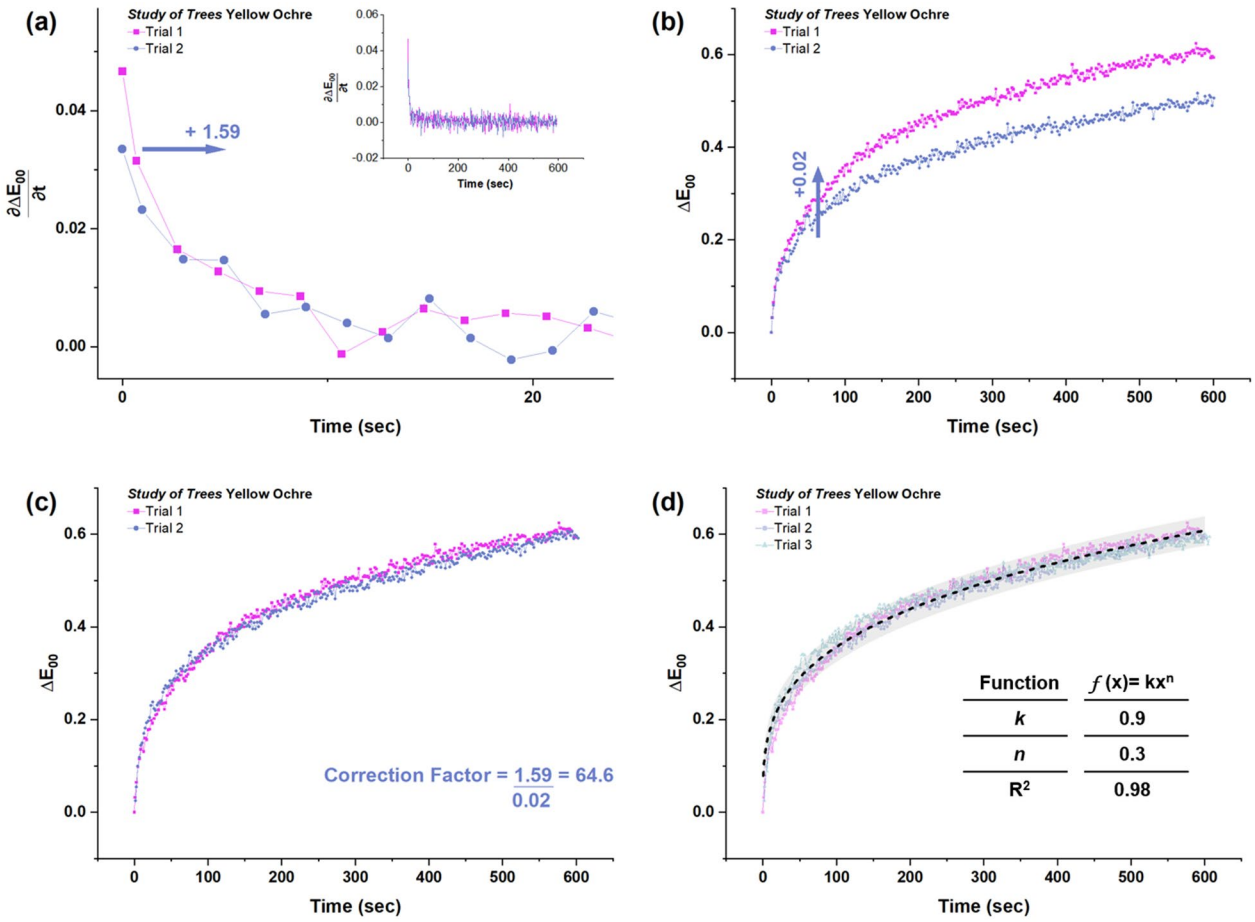

Fig. 9 Example of normalization procedure for MFT curves from, where **a** represents the shift in time obtained by taking the first derivative of each curve with respect to time, with the entirety of the differentiated curve illustrated in the inset. The next step in the correction, the shift in ΔE_{00} (y-axis) at 60 s, is illustrated in **b**. In **c**, the corrected curves are then superimposable, and **d** all three corrected curves are fitted to a concatenated power function

50–80 lx [55]. This understanding of the sensitivity of the carmine watercolors in *Foliage* and *Study of Trees* is useful for conservators and curatorial staff alike when planning the display and loan of these and similar works by Cezanne in the collection.

Further breaking down change by variable in the CIE L*a*b* color space shows some general trends for the pigments used by Cezanne (Fig. 11; the curves are illustrated in Additional file 1: Fig. S4). L* axis defines 0 as black and 100 as white, the a* axis reflects the green/red value, with negative values toward green and positive values towards red, and the b* axis represents the blue/yellow value, with negative numbers closer to blue and positive to yellow. The variable for chroma, or C, a function of a* and b*, is included here to better express the loss or gain of color saturation in polar space. The mean changes in L*a*b* and C observed at 600 s (ΔL, Δa, Δb, and ΔC) are illustrated in Fig. 12.

Overall, all colors will darken, loose saturation, and cool in tone, possibly predicting a future loss of contrast and vibrancy. The loss of saturation in the CIE L*a*b* color space signifies graying and future dulling with subsequent light exposure and most colors show negative ΔC values.

MFT predicts that *Study of Trees* will experience the most amount of change across all parameters although it shares a similar palette and support as in the case of *Foliage*. Examining the exhibition history for all three drawings reveals that until 2017, *Mont Sainte-Victoire* traveled between the donors of the drawing and MoMA and was offsite for a total of 31 years. From the documentation available since its acquisition in 1962, the drawing was on view for at least 33 months. *Foliage* and *Study of Trees* entered the collection in 1934. The object records generally do not specify which side was shown, but examining archival exhibition images indicate that only *Foliage*

Table 1 List of Colors and their corresponding absolute change (ΔE_{00}) and rate of change ($\frac{\partial \Delta E_{00}}{\partial t}$) values at 600 s

	Color	ΔE_{00}	$\frac{\partial \Delta E_{00}}{\partial t}$
Blue wool standards	BW1	3.6	0.0028
	BW2	1.7	0.0011
	BW3	0.7	$2.90E^{-4}$
Mont Sainte-Victoire (1902–06)	Paper	0.8	$5.60E^{-4}$
	Cobalt Blue	0.8	$6.30E^{-4}$
	Emerald Green	0.6	$4.00E^{-4}$
	Ochre	0.6	$3.90E^{-4}$
	Alizarin Lake	0.6	$4.40E^{-4}$
Foliage (1895)	Paper	0.9	$6.60E^{-4}$
	Cobalt Blue	0.5	$2.30E^{-4}$
	Emerald Green	0.4	$1.90E^{-4}$
	Ochre	0.5	$2.30E^{-4}$
	Carmine Lake	1.7	0.0012
Study of Trees (1895)	Paper	1.2	$8.30E^{-4}$
	Darkened Paper	1.1	$7.50E^{-4}$
	Ochre	0.6	$3.00E^{-4}$
	Carmine Lake	1.4	0.0013
	Vermilion	0.4	$1.30E^{-4}$

was shown. For this work, the record is comprehensive and includes the period before it entered the collection at MoMA; between 1907 and 2022, the drawing was on view for at least 78 months. Hagan et al. demonstrated that the light sensitivity of an object will decrease as it is exposed [56]. Therefore, the higher light sensitivity of *Study of Trees* might be related to the fact that it has not been exhibited, or at least, less frequently as the other two works.

A decrease in L*, which indicates darkening, was observed for both paper supports, though ultimately reaching a plateau (Additional file 1: Fig. S4). The paper used for *Foliage* and *Study of Trees* experienced more significant darkening in comparison with *Monte-Sainte Victoire*, which possibly speaks to the quality of the paper used by Cezanne in this instance. This darkening could have an overall effect on the sharpness of the composition and diminishes the appearance of thinner washes of color. The paper in both instances also showed a decrease in saturation and cooling (i.e., a decrease in C and b*, respectively). The loss of yellowness, or decrease in b*, could also represent a bleaching effect on the yellow chromophores in the aged paper. This effect was observed by Soleymani et al. for Japanese papers, where all papers aged with MFT exhibited varying degrees of bleaching, or decrease in b* [21].

Of all the watercolors, the carmine lake in *Foliage* and *Study of Trees* showed the largest degree of change in all CIE parameters and the trends indicate that the red colorant is likely to darken and discolor. Rader et al. observed that carminic acid used in a watercolor paint showed a decrease in absorbance in the green-yellow-red

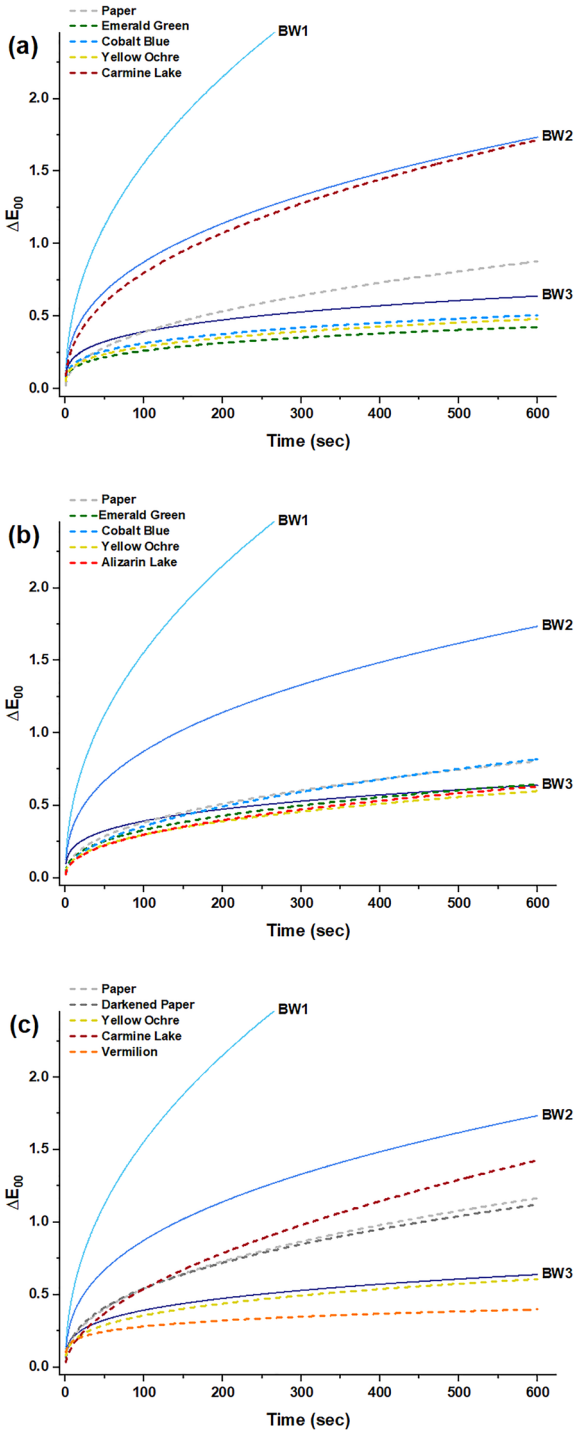

Fig. 10 All normalized and fitted MFT-induced color change (ΔE_{00}) curves for **a** *Mont Sainte-Victoire*, **b** *Foliage*, and **c** *Study of Trees*, alongside normalized and fitted BWS curves (BW1, 2, 3)

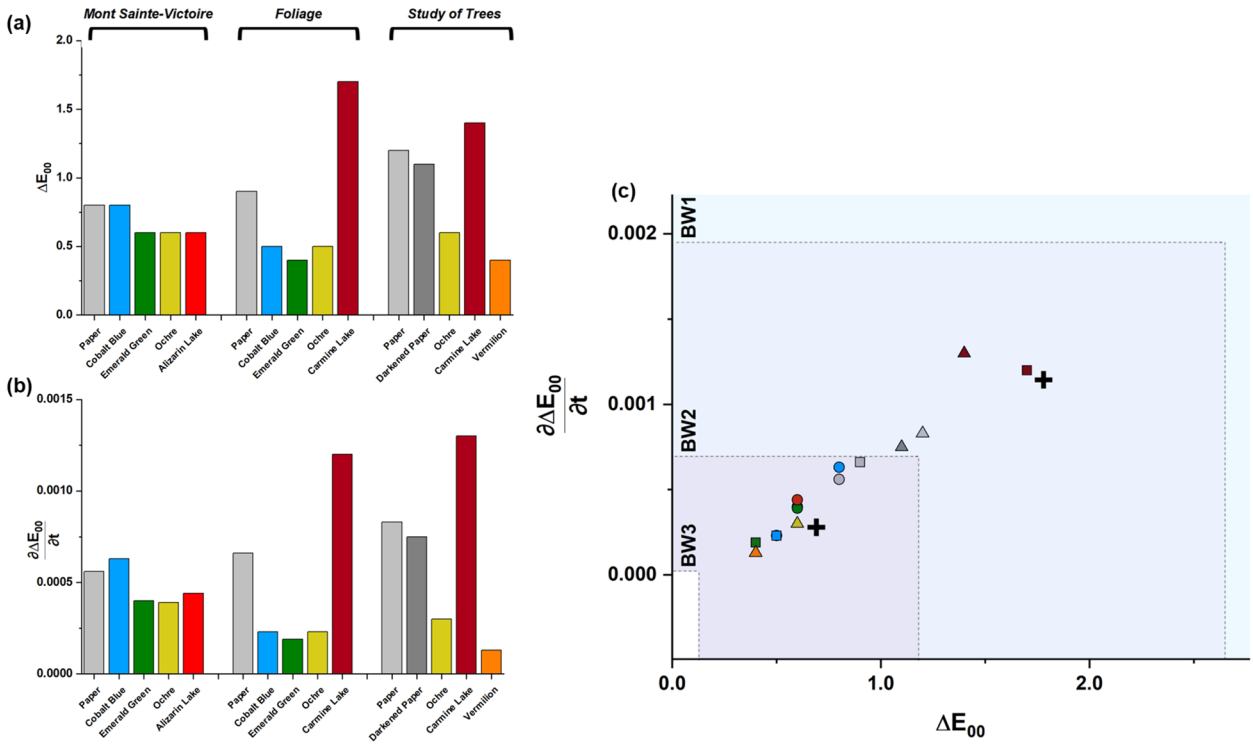

Fig. 11 MFT-induced color change (ΔE_{00}) (**a**) and rate of color change ($\frac{\partial \Delta E_{00}}{\partial t}$) (**b**) after 600 s. The two metrics are plotted as a function of the other in (**c**) with *Sainte-Victoire* (●), *Foliage* (▲), and *Study of Trees* (■). Dashed lines indicate the limits of the BWS categories as defined in Table 2. The fitted ΔE_{00} and $\frac{\partial \Delta E_{00}}{\partial t}$ for BW2 and BW3 are indicated by (+)

regions upon exposure to UV illumination [57]. This change is in line with the decrease in both a* and b* obtained with MFT that translates to green and blue shifts, respectively. This change has been previously attributed to light-induced ring opening reactions of the anthraquinone skeleton that lead to a breakdown of the chromophore and observed both in air and anoxic conditions [58].

In contrast, change was less prominent for the other reds, alizarin lake and vermilion. Alizarin lake has been reported as relatively stable in watercolors and was classified by Soleymani et al. as BW3, with changes due to reduction in lightness and increase in redness [21], similar to what was observed in *Mont Sainte-Victoire*. The most common discoloration for vermilion, or α-HgS, is blackening and was once thought to be exclusively caused by photoinduced structural change to black cubic β-HgS [59]. However, recent studies proved that the process is associated with Hg-Cl secondary products [60] that would go unmeasured by MFT alone. Vermilion blackening was not observed for the drawings investigated here.

Emerald green exhibited a shift towards red and darkening. All three compositions display degrees of discoloration and fading in the emerald green, particularly in dilute washes. Although copper acetoarsenite proved to be a more stable improvement on the older Scheele's green (copper arsenite), it was still reported to show browning in watercolors as early as 1888 [61, 62]. This phenomenon has been attributed most directly to the exposure of the emerald green in watercolors to sulfides, such as hydrogen sulfide (H_2S), which can react rapidly with the pigment to form copper sulfide (CuS) and induce a loss of chroma [36]. Other degradation pathways have been proposed for emerald green in oil paints, where oxidation of arsenic from As^{3+} to As^{5+} occurs with the formation of other arsenate species, such as calcium and lead, and results in marked browning [63, 64].

Yellow ochre appeared to darken and shift in tone towards blue-green with loss of saturation across all three drawings, although iron oxide and hydroxide pigments

Table 2 Upper and lower limits that define the change range for blue wool standards

	Absolute Change (ΔE_{00})	Rate of Change ($\frac{\partial \Delta E_{00}}{\partial t}$)
BW1	$4.5 \leq \Delta E_{00} \geq 2.7$	$3.7 \times 10^{-3} \leq \frac{\partial \Delta E_{00}}{\partial t} \geq 2.0 \times 10^{-3}$
BW2	$2.7 \leq \Delta E_{00} \geq 1.2$	$2.0 \times 10^{-3} \leq \frac{\partial \Delta E_{00}}{\partial t} \geq 7.0 \times 10^{-4}$
BW3	$1.2 \leq \Delta E_{00} \geq 0.1$	$7.0 \times 10^{-4} \leq \frac{\partial \Delta E_{00}}{\partial t} \geq 1.2 \times 10^{-4}$

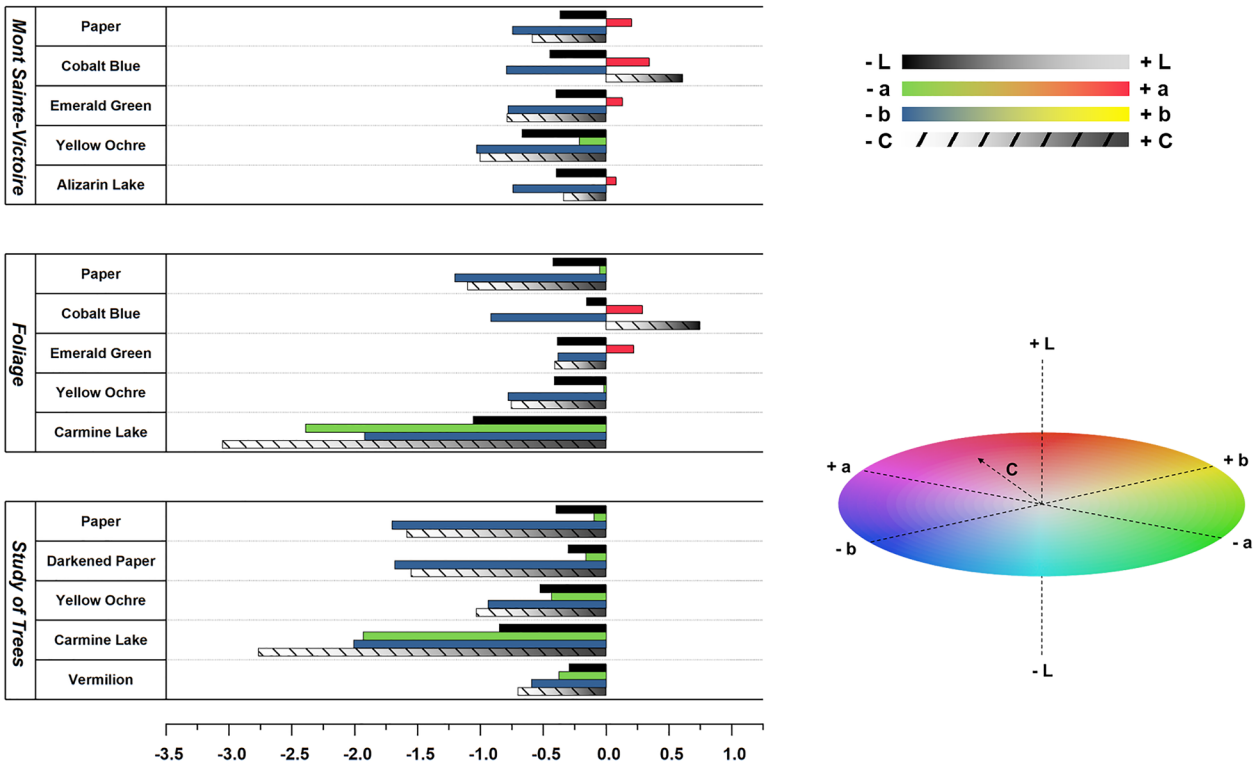

Fig. 12 ΔL, Δa, Δb, and ΔC for *Mont Sainte-Victoire*, *Foliage*, and *Study of Trees*, with CIE L*a*b* color space represented for reference

have long been considered permanent with stability to light and moisture, as well as basic and lightly acidic conditions [65]. And interestingly, the cobalt blues displayed positive ΔC values, or an increase in saturation. This, in combination with darkening and cooling in tone, could point towards a general deepening in tone and heightened contrast with future exposure. However, similar to ochres, cobalt blue has long been considered an entirely permanent pigment as far back as 1835, with only reports of discoloration in oil paints that are due to the interaction between the pigment and the medium that render the oil greenish-yellow [66].

Conclusion

Cezanne's palette for three of his mature watercolors in the MoMA collection was characterized by examination and scientific analysis. Most notably, the definitive identification of synthetic alizarin and carmine lakes is the first reporting of these pigments in watercolors by the artist, and the detection of rhodamine 6G further underscores the potential of scientific analysis to help with the dating of his oeuvre. The reds appear muted, and the emerald green, which Cezanne used extensively, showed browning in *Mont Sainte-Victoire* in particular, and thin washes have practically faded completely. Microfade testing offered further insight into the potential further shift of these colors. Overall, darkening was observed for all the colors and paper supports. The carmine red lake in *Foliage* and *Study of Trees* was the most sensitive of colors. Taken together, the analysis not only extended the knowledge of Cezanne's techniques and material choices but also clarified the condition and light sensitivity of these works. This reinforces the importance of following display guidelines that limit light exposure for these and similarly fugitive watercolors in Cezanne's oeuvre at MoMA and elsewhere.

Supplementary Information

The online version contains supplementary material available at https://doi.org/10.1186/s40494-023-00879-7.

Additional file 1: Table S1. The correction factors are listed for each color examined with MFT as per method described in ref. 54. **Figure S1.** Microfading curves obtained for *Monte Sainte Victoire*. **Figure S2**. Microfading curves obtained for *Foliage*. **Figure S3.** Microfading curves obtained for *Study of Trees*. **Figure S4.** Changes observed in ΔL, Δa, Δb, and ΔC for *Mont Sainte-Victoire* (●), *Foliage* (▲), and *Study of Trees* (■).

Acknowledgements

The authors thank Jodi Hauptman, Senior Curator; Samantha Friedman, Associate Curator; and Kiko Aebi, Curatorial Assistant, who organized the exhibition that prompted this research, and shared their expertise, enriching our understanding of the artist. Haddad is grateful for support from The David Booth Fellowship program in Conservation Science. Haddad and Martins

also acknowledge the generous guidance of Julio M del Hoyo-Meléndez and Marion Mecklenburg.

Author contributions
AH carried out p-XRF, XRF scanning, Raman, and SERS data acquisition and interpretation, in addition to MFT data interpretation. LN carried out UVF, and MFT. AH and LN prepared figures. AM aided with the interpretation of p-XRF, XRF scanning, and MFT data. All authors wrote and revised the main text and contributed to the study conceptualization. All authors have read and agreed to the published version of the manuscript. All authors read and approved the final manuscript.

Funding
This research received no external funding.

Availability of data and materials
The data is available on request.

Declarations

Competing interests
The authors declare no competing interests.

Received: 13 December 2022 Accepted: 8 February 2023
Published online: 24 February 2023

References

1. Gasquet J. Joachim Gasquet's Cezanne: a memoir with conversations. Reprint. London: Thames & Hudson; 1991.
2. Feilchenfeldt W, Warman J, Nash D. The paintings, watercolors and drawings of Paul Cézanne: an online catalogue Raisonné. https://www.cezannecatalogue.com/catalogue/index.php
3. Hauptman J, Friedman S, editors. Cézanne: drawing. New York: The Museum of Modern Art; 2021.
4. Ruppen F. Tackling Cezanne's Paper: on the reconstruction of loose sheets in Reconstructing Cézanne: Sequence and Process in Paul Cézanne's Works on Paper. London: Ridinghouse/Luxembourg & Dayan; 2022.
5. Neufeld L. Belle formule: materials and methods in Cézanne's watercolors. In: Hauptman J, Friedman S, editors. Cézanne Draw. New York: The Museum of Modern Art; 2021.
6. Russell WJ, de Abney WW, Britain G. Department of Science and Art Report to the Science and Art Department of the Committee of Council on Education on the action of light on water colours: presented to both Houses of Parliament by command of Her Majesty. London: Printed for HMSO by Eyre and Spottiswoode; 1888.
7. Brommelle NS. The Russell and Abney report on the action of light on water colours. Stud Conserv. 1964;9:140–52.
8. Michalski S. Agent of deterioration: light, ultraviolet and infrared. Gov. Can. 2018. https://www.canada.ca/en/conservation-institute/services/agents-deterioration/light.html.13 Dec 2022
9. Beltran VL, Druzik J, Maekawa S. Large-scale assessment of light-induced color change in air and anoxic environments. Stud Conserv Routledge. 2012;57:42–57.
10. Lerwill A, Townsend JH, Thomas J, Hackney S, Caspers C, Liang H. Photochemical colour change for traditional watercolour pigments in low oxygen levels. Stud Conserv. 2015;60:15–32.
11. Pullano M, Mårtensson M. Microfading of Watercolours by Carl Larsson from the Gothenburg Museum of Art. Sweden Stud Conserv. 2018;63:411–3.
12. Zieske F. An investigation of Paul Cézanne's watercolors with emphasis on emerald green. The Book and Paper Group of the American Institute for Conservation Annual. 1995;14.
13. Zieske F. Paul Cézanne's Watercolors: His Choice of Pigments and Papers. In: Stratis HK, Salvesen B, editors. The broad spectrum: studies in the materials, techniques, and conservation of color on paper. London: Archetype; 2002.
14. Reissner E. Ways of making: practice and innovation in Cézanne's paintings in the National Gallery. Natl Gallery Tech Bull. 2008;29:4–30.
15. Burnstock A, Reissner E, Richardson C, Van den Berg KJ. 2008 Analysis of Inorganic Materials from Paintings and Watercolours by Paul Cézanne from the Courtauld Gallery Using Two Methods of Non-Invasive Portable XRF with Light Microscopy and SEM/EDX Spectroscopy. 9th International Conference on NDT of Art: Jerusalem.
16. Butler M. An Investigation of the Materials and Technique Used by Paul Cézanne. 12th Annual Meeting of the American Institute for Conservation of Historic and Artistic Works: Preprints. Los Angeles. 1984
17. Butler S. Surface-Enhanced Raman Spectroscopy Studies Of Organic Dyes For Art Conservation And pH Sensing Applications [Master's Thesis]. Williamsburg, Virginia: The College of William & Mary; 2018.
18. Lerwill A, Brookes A, Townsend JH, Hackney S, Liang H. Micro-fading spectrometry: investigating the wavelength specificity of fading. Appl Phys A. 2015;118:457–63.
19. Jamison J, Davis S, Chemello C, Partridge W. A dionysian dilemma: the conservation and display of oversized Pompeian watercolors at the Kelsey museum of archaeology. The Book and Paper Group Annual. 2010;29:8.
20. Kogou S, Lucian A, Bellesia S, Burgio L, Bailey K, Brooks C, et al. A holistic multimodal approach to the non-invasive analysis of watercolour paintings. Appl Phys A. 2015;121:999–1014.
21. Soleymani S, Ireland T, McNevin D. Effects of Plant Dyes, Watercolors and Acrylic Paints on the Colorfastness of Japanese tissue papers. J Am Inst Conserv. 2016;55:56–70.
22. Solé VA, Papillon E, Cotte M, Walter Ph, Susini J. A multiplatform code for the analysis of energy-dispersive X-ray fluorescence spectra. Spectrochim Acta Part B At Spectrosc. 2007;62:63–8.
23. Alfeld M, Janssens K. Strategies for processing mega-pixel X-ray fluorescence hyperspectral data: a case study on a version of Caravaggio's painting Supper at Emmaus. J Anal At Spectrom. 2015;30:777–89.
24. Bell IM, Clark RJH, Gibbs PJ. Raman spectroscopic library of natural and synthetic pigments (pre- ≈ 1850 AD). Spectrochim Acta A Mol Biomol Spectrosc. 1997;53:2159–79.
25. Cañamares MV, Garcia-Ramos JV, Domingo C, Sanchez-Cortes S. Surface-enhanced Raman scattering study of the adsorption of the anthraquinone pigment alizarin on Ag nanoparticles: SERS study of alizarin adsorption on Ag nanoparticles. J Raman Spectrosc. 2004;35:921–7.
26. Pagliai M, Osticioli I, Nevin A, Siano S, Cardini G, Schettino V. DFT calculations of the IR and Raman spectra of anthraquinone dyes and lakes. J Raman Spectrosc. 2018;49:668–83.
27. Lux C, Lubio A, Ruediger A, Robert S, Muehlethaler C. Optimizing the analysis of dyes by surface-enhanced Raman Spectroscopy (SERS) using a conventional-microwave silver nanoparticles synthesis. Forensic Chem. 2019;16:100186.
28. Lunning E, Perkinson RL. The Print Council of America paper sample book: a practical guide to the description of paper. United States: Print Council of America; 1996.
29. Ruppen F. On Margins and Versos: the hidden relationships among Cézanne's works on paper. In: Eiling A, editor. Cézanne Metamorph. Karlsruhe: Prestel; 2017.
30. Julia de Fontenelle JSE, Poisson P. Manuel complet du marchand papetier et du régleur. Paris: Roret; 1828.
31. Sennelier G, de Catalogue général illustré G. Sennelier fabricant de couleurs fines et matériel d'artistes n° 7. Paris: Sennelier; 1896.
32. Lee SB, Bogaard J, Feller RL. Darkening of paper following exposure to visible and near-ultraviolet radiation. J Am Inst Conserv. 1989;28:1–18.
33. Banik G, Bruckle I. Paper and water: a guide for conservators. 1st ed. London: Butterworth-Heinemann; 2011.
34. Townsend JH, Carlyle L, Khandekar N, Woodcock S. Later nineteenth century pigments: evidence for additions and substitutions. Conservator. 1995;19:65–78.
35. Herm C. 2019 Emerald green versus Scheele's green: evidence and occurrence. Proceedings of the 7th interdisciplinary ALMA conference, Bratislava, Slovakia. 189–202.
36. Fielder I, Bayard M. Emerald Green and Scheele's Green. In: FitzHugh EW, editor. Artists' pigments: a handbook of their history and characteristics, vol. 3. Washington, DC: National Gallery of Art; 1997.
37. Reff T. Cézanne's constructive stroke. Art Q. 1962;25:3.

38. Prieto-Taboada N, Gómez-Laserna O, Martínez-Arkarazo I, Olazabal MÁ, Madariaga JM. Raman spectra of the different phases in the $CaSO_4$–H_2O system. Anal Chem. 2014;86:10131–7.
39. Schweppe H, Winter J. Madder and Alizarin. In: FitzHugh EW, editor. Artists' Pigments: a handbook of their history and characteristics, vol. 3. Washington, DC: National Gallery of Art; 1997.
40. Mairinger F, Banik G, Stachelberger H, Vendl A, Ponahlo J. The destruction of paper by green copper pigments, demonstrated by a sample of Chinese wallpaper. Stud Conserv. 1980;25:180–5.
41. Kirby J, Spring M, Higgitt C. The technology of eighteenth-and nineteenth-century red lake pigments. Natl Gallery Tech Bull. 2007;28:69.
42. Cooksey CJ. Quirks of dye nomenclature. 5 Rhodamines. Biotech Histochem. 2016;91:71–6.
43. Watanabe H, Hayazawa N, Inouye Y, Kawata S. DFT vibrational calculations of rhodamine 6G adsorbed on silver: analysis of tip-enhanced Raman spectroscopy. J Phys Chem B. 2005;109:5012–20.
44. Shabunya-Klyachkovskaya E, Vaschenko S, Stankevich V, Gaponenko S. The Identification of the Inorganic Pigments in the Cultural Heritage Objects Using Surface-Enhanced Raman Scattering. In: Di Bartolo B, Collins J, Silvestri L, editors. Nano-Structures for Optics and Photonics. Dordrecht: Springer; 2015. p. 467–9.
45. Hildebrandt P, Stockburger M. Surface-enhanced resonance Raman spectroscopy of rhodamine 6G adsorbed on colloidal silver. J Phys Chem. 1984;88:5935–44.
46. Kneipp K, Wang Y, Dasari RR, Feld MS. Approach to single molecule detection using surface-enhanced resonance raman scattering (SERRS): a study using rhodamine 6G on colloidal silver. Appl Spectrosc. 1995;49:780–4.
47. Kirby JO, Spring M, Higgitt C. The technology of red lake pigment manufacture: study of the dyestuff substrate. Natl Gallery Tech Bull. 2005;26:71–87.
48. Taylor JS, John S, Winsor & Newton. A descriptive handbook of modern water-colour pigments: illustrated with seventy-two colour washes skilfully gradated by hand on whatman's drawing paper : with an introductory essay on the recent water-colour controversy. London: Winsor & Newton; 1887.
49. Mecklenburg MF, del Hoyo-Meléndez JM. Development and application of a mathematical model to explain fading rate inconsistencies observed in light-sensitive materials: mathematical model to explain fading rate inconsistencies in light-sensitive materials. Color Technol. 2012;128:139–46.
50. Giles CH. The fading of colouring matters. J Appl Chem. 1965;15:541–50.
51. Daniels V. The light-fastness of textiles dyed with 6,6′-dibromoindigotin (Tyrian purple). J Photochem Photobiol Chem. 2006;184:73–7.
52. Prestel T. A classification system to enhance light-fastness data interpretation based on microfading tests and rate of colour change. Color Technol. 2017;133:506–12.
53. Druzik J, Pesme C. Comparison of Five Microfading Tester (MFT) Designs. The Textile Specialy Group Posprints; 2010.
54. Saunders D. Museum Lighting. Getty Publications: A Guide for Conservators and Curators; 2020.
55. Beltran VL, Pesme C, Feeman SK, Benson M. Microfading Tester: Light Sensitivity Assessment and Role in Lighting Policy. Los Angeles: J Paul Getty Trust; 2021.
56. Hagan E, Poulin J. The effect of prior exposure on the lightfastness of early synthetic dyes on textiles. Herit Sci. 2022;10:138.
57. Rader Bowers LM, Schmidtke Sobeck SJ. Impact of medium and ambient environment on the photodegradation of carmine in solution and paints. Dyes Pigments. 2016;127:18–24.
58. Koperska M, Łojewski T, Łojewska J. Vibrational spectroscopy to study degradation of natural dyes. assessment of oxygen-free cassette for safe exposition of artefacts. Anal Bioanal Chem. 2011;399:3271–83.
59. Miliani C, Monico L, Melo MJ, Fantacci S, Angelin EM, Romani A, et al. Photochemistry of Artists' Dyes and pigments: towards better understanding and prevention of colour change in works of art. Angew Chem Int Ed. 2018;57:7324–34.
60. Anaf W, Trashin S, Schalm O, van Dorp D, Janssens K, De Wael K. Electrochemical Photodegradation study of semiconductor pigments: influence of environmental parameters. Anal Chem. 2014;86:9742–8.
61. Banik G, Ponahlo J. Some aspects of degradation phenomena of paper caused by green copper-containing pigments. Pap Conserv. 1982;7:3–7.
62. Banik G. 1989 Discoloration of Green Copper Pigments in Manuscripts and Works of Graphic Art. Restaurator.
63. Keune K, Boon JJ, Boitelle R, Shimadzu Y. Degradation of Emerald green in oil paint and its contribution to the rapid change in colour of the *Descente des vaches* (1834–1835) painted by Théodore Rousseau. Stud Conserv. 2013;58:199–210.
64. Keune K, Mass J, Mehta A, Church J, Meirer F. Analytical imaging studies of the migration of degraded orpiment, realgar, and emerald green pigments in historic paintings and related conservation issues. Herit Sci. 2016;4:10.
65. Helwig K. Iron Oxide. In: Berrie B, editor. Artists' Pigments: a handbook of their history and characteristics, vol. 4. Washington, D.C: National Gallery of Art; 2007.
66. Roy A. Cobalt Blue. In: Berrie B, editor. Artists' Pigments: A Handbook of Their History and Characteristics, vol. 4. Washington, D.C: National Gallery of Art; 2007.

Publisher's Note